Inorganic Chemistry
Article

Inorg. Chem. **2009**, *48*, 10165–10176 **10165**
DOI: 10.1021/ic901148q

Synthesis, Structure, and Magnetic Characterization of a C_3-Symmetric $Mn^{III}_3Cr^{III}$ Assembly: Molecular Recognition Between a Trinuclear Mn^{III} Triplesalen Complex and a *fac*-Triscyano Cr^{III} Complex

Carl-Georg Freiherr von Richthofen,[†] Anja Stammler,[†] Hartmut Bögge,[†] Marty W. DeGroot,[‡] Jeffrey R. Long,[‡] and Thorsten Glaser*,[†]

[†]*Lehrstuhl für Anorganische Chemie I, Fakultät für Chemie, Universität Bielefeld, Universitätsstr. 25, D-33615 Bielefeld, Germany, and* [‡]*Department of Chemistry, University of California, Berkeley, 213A Lewis Hall, Berkeley, California 94720-1460*

Received June 15, 2009

The reaction of the tris(tetradentate) triplesalen ligand $H_6talen^{t\text{-}Bu_2}$, which provides three salen-like coordination environments bridged in a *meta*-phenylene arrangement by a phloroglucinol backbone, with Mn^{II} salts under aerobic conditions, affords, in situ, the trinuclear Mn^{III} triplesalen complex $[(talen^{t\text{-}Bu_2})\{Mn^{III}(solv)_n\}_3]^{3+}$. This species then reacts with $[(Me_3tacn)Cr(CN)_3]$ to form the tetranuclear complex $[\{(talen^{t\text{-}Bu_2})Mn^{III}_3\}\{(Me_3tacn)Cr(CN)_3\}]^{3+}$ ($[\mathbf{Mn^{III}_3Cr^{III}}]^{3+}$). The regular ligand folding observed in the trinuclear triplesalen complex preorganizes the three metal ions for the reaction with three facially coordinated nitrogen atoms of $[(Me_3tacn)Cr(CN)_3]$. $[\{(talen^{t\text{-}Bu_2})\text{-}(Mn^{III}(MeOH))_3\}\{(Me_3tacn)Cr(CN)_3\}](ClO_4)_3$ (**1**) was characterized by infrared spectroscopy, elemental analysis, mass spectrometry, electron absorption spectroscopy, and magnetic measurements. The molecular structure was established for the acetate-substituted derivative $[\{(talen^{t\text{-}Bu_2})(Mn^{III}(MeOH))_2(Mn^{III}(OAc))\}\{(Me_3tacn)Cr(CN)_3\}]\text{-}(ClO_4)_2$ (**2**) by single-crystal X-ray diffraction. Variable-temperature−variable-field and μ_{eff} versus T magnetic data have been analyzed in detail by full-matrix diagonalization of the appropriate spin-Hamiltonian, consisting of isotropic exchange, zero-field splitting, and Zeeman interaction components. Satisfactory reproduction of the experimental data has been obtained for the parameters $J_{Mn-Cr} = -0.12 \pm 0.04$ cm^{-1}, $J_{Mn-Mn} = -0.70 \pm 0.03$ cm^{-1}, and $D_{Mn} = -3.0 \pm 0.4$ cm^{-1}. These generate a triply degenerate pseudo $S_t = 7/2$ spin manifold, which cannot be appropriately described by a giant spin model and which exhibits a weak easy-axis magnetic anisotropy. This is corroborated by the onset of a frequency-dependent χ'' signal at low temperatures, demonstrating a slow relaxation of the magnetization indicative of **1** being a single-molecule magnet. Comparing the properties to those of the heptanuclear analogue $[\{(talen^{t\text{-}Bu_2})Mn^{III}_3\}_2\{Cr^{III}(CN)_6\}]^{3+}$ ($[\mathbf{Mn^{III}_6Cr^{III}}]^{3+}$) formed by the reaction of 2 equiv of $[(talen^{t\text{-}Bu_2})\{Mn^{III}(solv)_n\}_3]^{3+}$ with 1 equiv of $[Cr(CN)_6]^{3-}$ [Glaser, T.; Heidemeier, M.; Weyhermüller, T.; Hoffmann, R.-D.; Rupp, H.; Müller, P. *Angew. Chem. Int. Ed.*, 2006, **45**, 6033−6037] demonstrates a lower driving force for formation, a strongly reduced J_{Mn-Cr} exchange, a slightly reduced J_{Mn-Mn} exchange, and a significantly longer $Mn-N^{N\equiv C}$ bond length in $[\mathbf{Mn^{III}_3Cr^{III}}]^{3+}$. Taking into account magneto-structural correlations establishes a supramolecular interaction between the two $[(talen^{t\text{-}Bu_2})Mn^{III}_3]^{3+}$ subunits in $[\mathbf{Mn^{III}_6Cr^{III}}]^{3+}$ responsible for the structural distortion and the short $Mn-N^{N\equiv C}$ distance which results in a strong J_{Mn-Cr} exchange and thus $[\mathbf{Mn^{III}_6Cr^{III}}]^{3+}$ being a single-molecule magnet with a relatively high effective anisotropy barrier of 25.4 K.

1. Introduction

The design and synthesis of molecule-based magnets has attracted considerable interest over the past decades.[1−3] Beyond the synthesis of magnetic materials based on molecular entities that exhibit a spontaneous long-range ferromagnetic ordering, the observation that the molecular complex $[\mathbf{Mn_{12}}O_{12}(O_2CCH_3)_{16}(OH_2)_4]$, $\mathbf{Mn_{12}}$,[4] exhibits a hysteresis in the magnetization of purely molecular origin[5,6] opened the field to a new class of molecular magnetic materials called

*To whom correspondence should be addressed. E-mail: thorsten.glaser@uni-bielefeld.de.

(1) Miller, J. S.; Epstein, A. J. In *Molecular Magnetism: From Molecular Assemblies to the Devices*; Coronado, E., Delhaes, P., Gatteschi, D., Miller, J. S., Eds.; NATO ASI Series, Series E: Dordrecht, The Netherlands, 1995; Vol. *321*; pp 379−414.
(2) Miller, J. S.; Epstein, A. J.; Reiff, W. M. *Acc. Chem. Res.* **1988**, *21*, 114–120.
(3) Miller, J. S. *Inorg. Chem.* **2000**, *39*, 4392–4408.
(4) Lis, T. *Acta Crystallogr.* **1980**, *36*, 2042–2046.
(5) Sessoli, R.; Gatteschi, D.; Caneschi, A.; Novak, M. A. *Nature* **1993**, *365*, 141–143.
(6) Sessoli, R.; Tsai, H. L.; Schake, A. R.; Wang, S. Y.; Vincent, J. B.; Folting, K.; Gatteschi, D.; Christou, G.; Hendrickson, D. N. *J. Am. Chem. Soc.* **1993**, *115*, 1804–1816.

Published on Web 10/05/2009

single-molecule magnets (SMMs).[7−10] SMMs possess a superior property in comparison to other paramagnetic polynuclear transition metal complexes: SMMs can be magnetized and retain their polarization in the absence of an external magnetic field. Accordingly, they exhibit a hysteresis in the magnetization in analogy to solid-state magnets. Due to these promising properties, SMMs have attracted a great deal of research attention since their discovery in 1993. Despite the report of an ever increasing number of new SMMs, a key property, the effective energy barrier for magnetization reversal, has only recently been increased moderately in comparison to Mn_{12} by a class of complexes abbreviated **Mn_6** (= $[Mn^{III}{}_6O_2(R^1sao)_6(O_2CR^2)_2(R^3OH)_4]$ with H_2R^1sao = salicylaldoxime).[11−15] One reason that progress has been difficult is the serendipitous nature of most approaches[16] employed to generate new SMMs:[17] appropriate metal ions and bridging ligands are reacted without knowing the resulting molecular structure of the product but with the hope to obtain a new SMM. However, the intensive research on SMMs provided some key recipes for a more rational approach to constructing SMMs: the design of a SMM requires not only the realization of a high-spin ground state S_t and a source of magnetic anisotropy but also a control of the molecular topology. In order to minimize the quantum mechanical magnetization tunneling, the complex should be at least C_3 symmetric, but the symmetry should be lower than cubic to ensure the presence of a unique axis along which magnetic anisotropy can develop.

We have been able to incorporate these requirements in a rational ligand[18−21] and complex design, resulting in the heptanuclear SMM $[\{(talen^{t\text{-}Bu_2})Mn^{III}\}_3\{Cr^{III}(CN)_6\}]^{3+}$ (**$[Mn^{III}{}_6Cr^{III}]^{3+}$**; note that the weakly bound solvent molecules on the sixth coordination sites of some of the Jahn−Teller distorted Mn^{III} ions have been neglected in this formulation),[22] which is assembled from three molecular building blocks (Scheme 1, left). Two bowl-shaped[20,23−25] tricationic Mn^{III} complexes $[(talen^{t\text{-}Bu_2})\{Mn^{III}(solv)_n\}_3]^{3+}$ of the triplesalen ligand $H_6talen^{t\text{-}Bu_2}$ react with one trianionic $[Cr(CN)_6]^{3-}$ complex as a hexaconnector. This reaction is based on the long-established success of the combination of metal salen units with hexacyanometallates[8,26−36] and the highly predictable exchange coupling through cyanide bridges.[31,37−39] It has been demonstrated, for example, that even a trinuclear complex constructed from two Mn^{III} salen complexes bridged through a central $[Fe(CN)_6]^{3-}$ complex can act as a SMM due to the ferromagnetic S_t = 9/2 spin ground state, the local magnetic anisotropy of the Mn^{III} salen units, and the linear topology.[40−42]

The advantage of our trinuclear building block $[(talen^{t\text{-}Bu_2})\{Mn^{III}(solv)_n\}_3]^{3+}$ is the ligand folding, which preorganizes the three Mn^{III} ions for coordination of three facial nitrogen atoms of a hexacyanometallate $[M(CN)_6]^{n-}$ and should therefore result in a driving force for the formation of heptanuclear complexes **$[M^t{}_6M^c]^{n+}$** (M^t = terminal metal ion of the triplesalen building block; M^c = central metal ion of the hexacyanometallate) by molecular recognition (Scheme 1, left). We have shown that the formation of **$[Mn^{III}{}_6Cr^{III}]^{3+}$** was not a singularity but that the molecular recognition by the preorganization of the three molecular building blocks in analogy to the key−lock principle provides a strong driving force for the generation of heptanuclear complexes of the general formula **$[M^t{}_6M^c]^{n+}$**. The reaction of $[(talen^{t\text{-}Bu_2})\{Mn^{III}(solv)_n\}_3]^{3+}$ with $[Fe(CN)_6]^{3-}$ resulted in the formation of $[\{(talen^{t\text{-}Bu_2})Mn^{III}{}_3\}_2\{Fe^{III}(CN)_6\}]^{3+}$ (**$[Mn^{III}{}_6Fe^{III}]^{3+}$**) isolated as its $[Fe(CN)_6]^{3-}$ salt.[43]

(7) Christou, G.; Gatteschi, D.; Hendrickson, D. N.; Sessoli, R. *MRS Bull.* **2000**, *25*, 66–71.
(8) Long, J. R. In *Chemistry of Nanostructured Materials*; Yang, P., Ed.; World Scientific: Hong Kong, 2003; pp 291−315.
(9) Gatteschi, D.; Sessoli, R. *Angew. Chem., Int. Ed.* **2003**, *42*, 268–297.
(10) Gatteschi, D.; Sessoli, R.; Villain, J. *Molecular Nanomagnets*; Oxford University Press: Oxford, U. K., 2006.
(11) Milios, C. J.; Vinslava, A.; Wernsdorfer, W.; Moggach, S.; Parsons, S.; Perlepes, S. P.; Christou, G.; Brechin, E. K. *J. Am. Chem. Soc.* **2007**, *129*, 2754–2755.
(12) Milios, C. J.; Inglis, R.; Bagai, R.; Wernsdorfer, W.; Collins, A.; Moggach, S.; Parsons, S.; Perlepes, S. P.; Christou, G.; Brechin, E. K. *Chem. Comm.* **2007**, 3476–3478.
(13) Milios, C. J.; Inglis, R.; Vinslava, A.; Bagai, R.; Wernsdorfer, W.; Parsons, S.; Perlepes, S. P.; Christou, G.; Brechin, E. K. *J. Am. Chem. Soc.* **2007**, *129*, 12505–12511.
(14) Piligkos, S.; Bendix, J.; Milios, C. J.; Brechin, E. K. *Dalton Trans.* **2008**, 2277–2284.
(15) Prescimone, A.; Milios, C. J.; Moggach, S.; Warren, J. E.; Lennie, A. R.; Sanchez-Benitez, J.; Kamenev, K.; Bircher, R.; Murrie, M.; Parsons, S.; Brechin, E. K. *Angew. Chem., Int. Ed.* **2008**, *47*, 2828–2831.
(16) Winpenny, R. E. P. *J. Chem. Soc., Dalton Trans.* **2002**, 1–10.
(17) Aromi, G.; Brechin, E. K. *Struct. Bonding* (*Berlin*) **2006**, *122*, 1–67.
(18) Glaser, T.; Gerenkamp, M.; Fröhlich, R. *Angew. Chem., Int. Ed.* **2002**, *41*, 3823–3825.
(19) Glaser, T.; Heidemeier, M.; Lügger, T. *Dalton Trans.* **2003**, 2381–2383.
(20) Glaser, T.; Heidemeier, M.; Fröhlich, R.; Hildebrandt, P.; Bothe, E.; Bill, E. *Inorg. Chem.* **2005**, *44*, 5467–5482.
(21) Glaser, T.; Heidemeier, M.; Grimme, S.; Bill, E. *Inorg. Chem.* **2004**, *43*, 5192–5194.
(22) Glaser, T.; Heidemeier, M.; Weyhermüller, T.; Hoffmann, R.-D.; Rupp, H.; Müller, P. *Angew. Chem., Int. Ed.* **2006**, *45*, 6033–6037.
(23) Glaser, T.; Heidemeier, M.; Strautmann, J. B. H.; Bögge, H.; Stammler, A.; Krickemeyer, E.; Huenerbein, R.; Grimme, S.; Bothe, E.; Bill, E. *Chem.—Eur. J.* **2007**, *13*, 9191–9206.
(24) Glaser, T.; Heidemeier, M.; Fröhlich, R. *Compt. Rend. Chim.* **2007**, *10*, 71–78.
(25) Theil, H.; Frhr. v. Richthofen, C.-G.; Stammler, A.; Bögge, H.; Glaser, T. *Inorg. Chim. Acta* **2008**, *361*, 916–924.
(26) Miyasaka, H.; Matsumoto, N.; Okawa, H.; Re, N.; Gallo, E.; Floriani, C. *J. Am. Chem. Soc.* **1996**, *118*, 981–994.
(27) Re, N.; Gallo, E.; Floriani, C.; Miyasaka, H.; Matsumoto, N. *Inorg. Chem.* **1996**, *35*, 6004–6008.
(28) Miyasaka, H.; Ieda, H.; Matsumoto, N.; Re, N.; Crescenzi, R.; Floriani, C. *Inorg. Chem.* **1998**, *37*, 255–263.
(29) Re, N.; Crescenzi, R.; Floriani, C.; Miyasaka, H.; Matsumoto, N. *Inorg. Chem.* **1998**, *37*, 2717–2722.
(30) Miyasaka, H.; Matsumoto, N.; Re, N.; Gallo, E.; Floriani, C. *Inorg. Chem.* **1997**, *36*, 670–676.
(31) Verdaguer, M.; Bleuzen, A.; Marvaud, V.; Vaissermann, J.; Seuleiman, M.; Desplanches, C.; Scuiller, A.; Train, C.; Garde, R.; Gelly, G.; Lomenech, C.; Rosenman, I.; Veillet, P.; Cartier, C.; Villain, F. *Coord. Chem. Rev.* **1999**, *190−192*, 1023–1047.
(32) Ohba, M.; Okawa, H. *Coord. Chem. Rev.* **2000**, *198*, 313–328.
(33) Beltran, L. M. C.; Long, J. R. *Acc. Chem. Res.* **2005**, *38*, 325–334.
(34) Rebilly, J.-N.; Mallah, T. *Struct. Bonding* (*Berlin*) **2006**, *122*, 103–131.
(35) Schelter, E. J.; Prosvirin, A. V.; Dunbar, K. R. *J. Am. Chem. Soc.* **2004**, *126*, 15004–15005.
(36) Palii, A. V.; Ostrovsky, S. M.; Klokishner, S. I.; Tsukerblat, B. S.; Berlinguette, C. P.; Dunbar, K. R.; Galán-Mascarós, J. R. *J. Am. Chem. Soc.* **2004**, *126*, 16860–16867.
(37) Dunbar, K. R.; Heintz, R. A. *Prog. Inorg. Chem.* **1997**, *45*, 283–391.
(38) Weihe, H.; Güdel, H. U. *Comments Inorg. Chem* **2000**, *1−2*, 75.
(39) Atanasov, M.; Comba, P.; Daul, C. A. *J. Phys. Chem. A* **2006**, *110*, 13332–13340.
(40) Choi, H. J.; Sokol, J. J.; Long, J. R. *Inorg. Chem.* **2004**, *43*, 1606–1608.
(41) Ferbinteanu, M.; Miyasaka, H.; Wernsdorfer, W.; Nakata, K.; Sugiura, K.-i.; Yamashita, M.; Coulon, C.; Clerac, R. *J. Am. Chem. Soc.* **2005**, *127*, 3090–3099.
(42) Tregenna-Piggott, P. L. W.; Sheptyakov, D.; Keller, L.; Klokishner, S. I.; Ostrovsky, S. M.; Palii, A. V.; Reu, O. S.; Bendix, J.; Brock-Nannestad, T.; Pedersen, K.; Weihe, H.; Mutka, H. *Inorg. Chem.* **2009**, *48*, 128–137.
(43) Glaser, T.; Heidemeier, M.; Krickemeyer, E.; Bögge, H.; Stammler, A.; Fröhlich, R.; Bill, E.; Schnack, J. *Inorg. Chem.* **2009**, *48*, 607–620.

Scheme 1. (Left) Building Block Approach for the Successful Construction of Heptanuclear Complexes $[\mathbf{M'_6M^c}]^{n+}$,[a] (Right) Adaption of This Building Block Approach for the Construction of Tetranuclear Complexes $[\mathbf{M'_3M^c}]^{n+}$ by Substitution of Three *fac*-Cyanides of a Hexacyanometallate by a Facially Coordinated Blocking Ligand, and (Bottom) Identity of the Bowl-Shaped Molecular Building Block $[(\text{talen}^{t\text{-Bu}_2})\{\text{Mn}^{\text{III}}(\text{solv})_n\}_3]^{3+}$

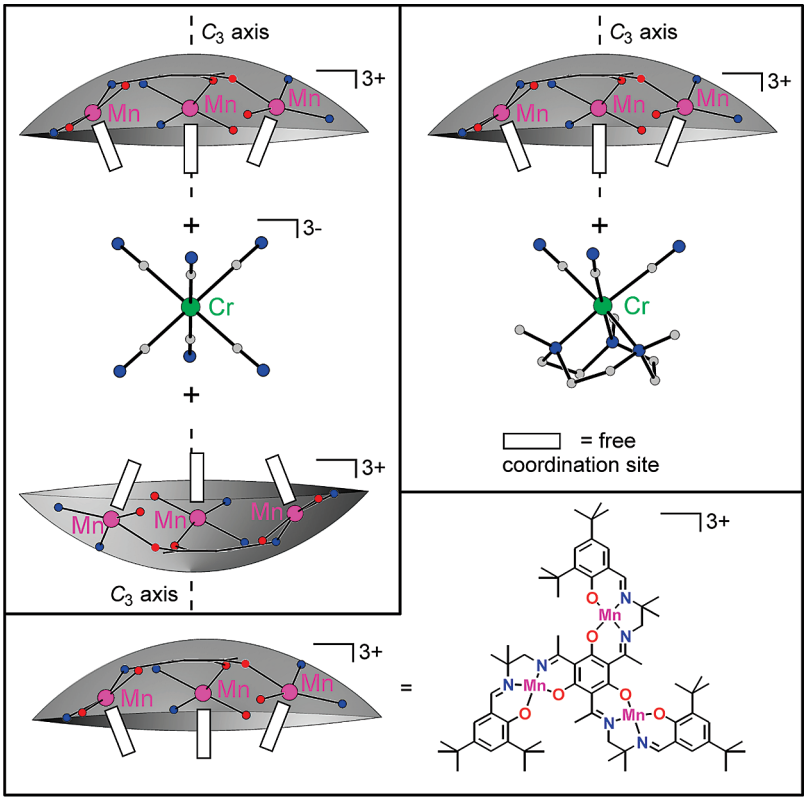

[a] The bowl-shaped structure of the trinuclear triplesalen building block preorganizes the three metal ions for coordination to the N atoms of a hexacyanometallate. This molecular recognition provides a driving force for the formation of the heptanuclear complex in analogy to the key−lock principle.

Magnetic measurements established $[\mathbf{Mn^{III}_6Cr^{III}}]^{3+}$ to be a SMM[22] and $[\mathbf{Mn^{III}_6Fe^{III}}]^{3+}$ not to be a SMM.[43] Due to the large Hilbert space (62 500), the analysis of the magnetic data for $[\mathbf{Mn^{III}_6Cr^{III}}]^{3+}$ (temperature-dependent magnetization data at 1 T and variable-temperature−variable-field (VTVH) magnetization data at 1, 4, and 7 T) has only been performed with a spin-Hamiltonian consisting of an isotropic Heisenberg−Dirac−van Vleck (HDvV) term and a Zeeman term. In addition, due to the neglect of zero-field splitting terms, only data above 50 K have been used to obtain the exchange coupling parameters.[22] On the other hand, for $[\mathbf{Mn^{III}_6Fe^{III}}]^{3+}$, we were able to obtain reliable values for the exchange coupling constants J_{ij} and the local magnetic anisotropies D_i, by analyzing the magnetic data with the appropriate spin-Hamiltonian including HDvV, zero-field splitting, and Zeeman terms by full-matrix diagonalization. The relative orientations of the local D_i tensors have been incorporated by employing the local Jahn−Teller axes of the Mn^{III} ions.[43]

The coupling between the Mn^{III} ions in a trinuclear Mn^{III} triplesalen building block is slightly antiferromagnetic in both heptanuclear complexes and not, as in the case of the trinuclear Cu^{II}[18,21,23] and $V^{IV}{=}O$[25] complexes, ferromagnetic ($[\mathbf{Mn^{III}_6Cr^{III}}]^{3+}$, $J_{\text{Mn-Mn}} = -1.0\ \text{cm}^{-1}$; $[\mathbf{Mn^{III}_6Fe^{III}}]^{3+}$, $J_{\text{Mn-Mn}} = -0.9\ \text{cm}^{-1}$). The coupling of the Mn^{III} ions with the Cr^{III} ions of the bridging hexacyanochromate in $[\mathbf{Mn^{III}_6Cr^{III}}]^{3+}$[22] was also found to be antiferromagnetic with $J_{\text{Cr-Mn}} = -5.0\ \text{cm}^{-1}$. This results in the stabilization of a high-spin ground state of $S_t = 21/2$. On the other hand, the ferromagnetic but small coupling of $J_{\text{Fe-Mn}} = +0.7\ \text{cm}^{-1}$ established in $[\mathbf{Mn^{III}_6Fe^{III}}]^{3+}$ between the terminal Mn^{III} ions and the central low-spin Fe^{III} ion results in a strong mixing of m_S wave functions of various spin states, so that a description with total spin states S_t is not appropriate. Thus, the reason for $[\mathbf{Mn^{III}_6Cr^{III}}]^{3+}$ being a SMM and for $[\mathbf{Mn^{III}_6Fe^{III}}]^{3+}$ not being a SMM is the strong $J_{\text{Cr-Mn}}$ coupling in comparison to the small $J_{\text{Fe-Mn}}$ coupling. The relatively strong zero-field splitting established for the Mn^{III} ions in $[\mathbf{Mn^{III}_6Fe^{III}}]^{3+}$ of $D_{\text{Mn}} = -(3.0 \pm 0.7)\ \text{cm}^{-1}$ proves the validity of the design concept.[19,21]

In order to (*i*) test the principle driving force by molecular recognition/electrostatic attraction, (*ii*) change the overall symmetry and thus the relative orientation of the local anisotropy tensors, and (*iii*) simplify the analysis of the magnetic measurements by reducing the Hilbert space, we have used the well-established building block $[(\text{Me}_3\text{tacn})\text{Cr}(\text{CN})_3]$[44] as a *half-unit* of $[\text{Cr}(\text{CN})_6]^{3-}$ to synthesize the C_3-symmetric tetranuclear complex $[\{(\text{talen}^{t\text{-Bu}_2})\text{Mn}^{\text{III}}{}_3\}\{(\text{Me}_3\text{tacn})\text{Cr}(\text{CN})_3\}]^{3+}$ ($[\mathbf{Mn^{III}_3Cr}]^{3+}$, Scheme 1, right). Here, we report its synthesis, structure, and magnetic characterization.

2. Experimental Section

2.1. Preparation of Compounds. $H_6\text{talen}^{t\text{-Bu}_2}$ { = 2,4,6-tris{1-[2-(3,5-di-*tert*-butylsalicylaldimino)-2-methylpropylimino]-ethyl}-1,3,

(44) Berseth, P. A.; Sokol, J. J.; Shores, M. P.; Heinrich, J. L.; Long, J. R. *J. Am. Chem. Soc.* **2000**, *122*, 9655–9662.

5-trihydroxybenzene}[19,20] and [(Me_3tacn)Cr($CN)_3$][44] were synthesized as described previously.

[{(talen$^{t\text{-}Bu_2}$)(Mn^{III}(MeOH))$_3$}{(Me_3tacn)Cr($CN)_3$}]($ClO_4)_3$ (1). A solution of 162 mg (0.448 mmol) of $Mn(ClO_4)_2 \cdot 6H_2O$ in methanol (20 mL) was added to a stirred suspension of 164 mg (0.148 mmol) of H_6talen$^{t\text{-}Bu_2}$ in methanol (20 mL). After the addition of a solution of 84 mg (0.83 mmol) of NEt_3 in methanol (5 mL), the mixture was heated to reflux for 20 min, resulting in a brown solution. The reaction solution was allowed to cool to room temperature and was stirred for 2 h in an open flask. After adding dropwise a solution of 45 mg (0.15 mmol) of [(Me_3tacn)Cr($CN)_3$] in methanol (16 mL), the reaction mixture was stirred at room temperature for 1.5 h. The solution was filtered and treated with a solution of 140 mg (0.997 mmol) of $NaClO_4 \cdot H_2O$ in methanol (10 mL). Upon the slow diffusion of *tert*-butyl methyl ether into the reaction solution, brownish-black needles were obtained, which were analyzed as $\mathbf{1} \cdot 4H_2O$. Yield: 115 mg (38%). ESI-MS (CH_3CN): *m*/*z* 523.9 [{(talen$^{t\text{-}Bu_2}$)-Mn_3}{(Me_3tacn)Cr($CN)_3$}]$^{3+}$. IR (KBr): ν 2955m, 2908w, 2870w, 2153vw, 1613m, 1562m, 1537m, 1487s, 1393m, 1366w, 1277m, 1120m, 1084m,1003w, 978w, 847w, 625w, 581w. Elem anal. (%) calcd for $\mathbf{1} \cdot 4H_2O$ ($C_{84}H_{137}N_{12}O_{25}Cl_3Mn_3Cr$): C, 49.50; H, 6.77; N, 8.24. Found: C, 49.49; H, 6.52; N, 8.35.

Under the same protocol but using manganese(II)acetate/$NaClO_4$ instead of manganese(II)perchlorate/NEt_3, an inhomogeneous powder in conjunction with a few single crystals of $\mathbf{2} \cdot 5$MeOH as a minor component suited for X-ray diffraction have been obtained. As no pure sample of **2** has been obtained either from modifications of the reaction conditions or by recrystallization, we refrain from further characterization.

2.2. X-Ray Crystallography. Crystals of $\mathbf{2} \cdot 5$MeOH were removed from the mother liquor and immediately cooled to 183(2) K on a Bruker AXS SMART diffractometer (three circle goniometer with 1 K CCD detector, Mo Kα radiation, detector distance 5 cm). A total of 48 084 reflections ($1.80 < \Theta < 25.00°$) were collected, of which 18 985 reflections were unique (R(int) = 0.0287). $C_{90}H_{148}Cl_2CrMn_3N_{12}O_{23}$, M = 2053.92 g mol^{-1}, triclinic, space group $P\bar{1}$, a = 15.6351(6), b = 17.3305(7), c = 21.2534(8) Å, α = 80.189(1), β = 72.909(1), γ = 89.786(1)°, V = 5417.5(4) Å^3, Z = 2, ρ = 1.259 g cm^{-3}, μ = 0.558 mm^{-1}. Empirical absorption correction with SADABS 2.10.[45] The structure was solved using SHELXS-97[46] and refined using SHELXL-97[46,47] to R = 0.0519 for 16 235 reflections with $I > 2\sigma(I)$, R = 0.0617 for all reflections; max/min residual electron density = 0.725/−0.629 e Å^{-3}.

Several attempts to perform a single-crystal structure analysis of **1** were made. Inspection of the CCD frames showed a strong decrease of intensity with increasing diffraction angle and often split reflections, indicating disorder and twinning. The best investigated crystal at least allowed the clear detection of all atoms of two crystallographically independent complexes in the unit cell, the corresponding six ClO_4^- counteranions, and some disordered solvent molecules. Results: monoclinic, space group $P2_1/c$, a = 22.654, b = 39.108, c = 30.133 Å, β = 92.64°, Z = 8.

2.3. Other Physical Measurements. Temperature-dependent magnetic susceptibilities were measured on powdered samples of **1** by using a SQUID magnetometer (Quantum Design MPMS XL-7 EC) at 1.0 T (2.0−300K). VTVH measurements were performed at 0.5, 1, 2, 3, 5, and 7 T in the range 2−10 K with the magnetization equidistantly sampled on a $1/T$ temperature scale. The ac susceptibility measurements were performed in an oscillating ac field with an amplitude of 3 Oe and 0 dc field. The oscillation frequencies were 633.5, 910.2, 1186.7, and 1464.8 Hz. For calculation of the molar magnetic susceptibilities, χ_M, the measured susceptibilities were corrected for the underlying diamagnetism of the sample holder and the sample by using tabulated Pascal's constants. The program package JulX was used for spin-Hamiltonian simulations and fittings of the data by a full-matrix diagonalization approach.[48] Infrared spectra (400−4000 cm^{-1}) of solid samples were recorded on a Shimadzu FTIR 8300 as KBr disks. UV/vis/NIR absorption spectra of solutions were measured on a Shimadzu UV3101PC spectrophotometer in the range 190−3200 nm at ambient temperatures. ESI mass spectra were recorded on an Esquire 3000 ion trap mass spectrometer (Bruker Daltonik GmbH, Bremen, Germany).

3. Results and Analysis

3.1. Synthesis and Characterization. The syntheses of the heptanuclear triplesalen complexes $[\mathbf{Mn_6M}]^{3+}$ usually employ the molecular building block [(talen$^{t\text{-}Bu_2}$){Mn^{III}-(solv)$_n$}$_3$]$^{3+}$, which is generated in situ by reacting the ligand H_6talen$^{t\text{-}Bu_2}$ with manganese(II)acetate, manganese-(II)lactate, or manganese(II)perchlorate/NEt_3 in methanol under reflux and aerobic oxidation. The resulting brown solution of [(talen$^{t\text{-}Bu_2}$){Mn^{III}(solv)$_n$}$_3$]$^{3+}$ is then treated with a solution containing the hexacyanometallate anion. This procedure in methanol usually provides the heptanuclear complexes $[\mathbf{Mn_6M}]^{3+}$ in good yield by crystallization.[22,43,49]

The application of this procedure to the preparation of $[\mathbf{Mn_3Cr}]^{3+}$ was not straightforward. Crystallization by simple concentration of the reaction solution did not work, and diffusion of the solvents, in which the resulting complex is insoluble, was necessary. However, the yields were lower in comparison to those observed for the heptanuclear complexes. A reproducible synthesis was obtained for [{(talen$^{t\text{-}Bu_2}$)(Mn^{III}(MeOH))$_3$}{(Me_3tacn)-Cr($CN)_3$}]($ClO_4)_3$ (**1**) starting from manganese(II)-perchlorate/NEt_3. Single crystals obtained by the diffusion of *tert*-butyl methyl ether into the reaction solutions had severe twinning problems that denied a complete refinement. However, the molecular structures of two independent but structurally very similar [(talen$^{t\text{-}Bu_2}$)-(Mn^{III}(MeOH))$_3$]$^{3+}$ complexes could be established. Single crystals suitable for complete crystal structure refinement were obtained by employing manganese-(II)acetate, with the addition of $NaClO_4$ and diffusion of diethyl ether into the reaction solution. However, these single crystals were only obtained as a side product to an inhomogeneous powder that prevented us from performing a complete characterization. Single-crystal X-ray diffraction established the formulation [{(talen$^{t\text{-}Bu_2}$)-(Mn^{III}(MeOH))$_2$(Mn^{III}(OAc))}{(Me_3tacn)Cr($CN)_3$}]($ClO_4)_2 \cdot$ 5MeOH ($\mathbf{2} \cdot 5$MeOH), wherein one coordinated methanol molecule is substituted by an acetate anion, reducing the overall charge to a dication.

Another problem in the synthesis of $[\mathbf{Mn_3Cr}]^{3+}$ emerged from the very low intensity of the CN stretching vibration. The FTIR spectra of triplesalen complexes are dominated by vibrations due to the ligand skeleton, and these show only minor variations for the free ligand H_6talen$^{t\text{-}Bu_2}$,[19,20] trinuclear complexes [(H_6talen$^{t\text{-}Bu_2}$)M_3]$^{n+}$,[20,23,49] and heptanuclear

(45) Sheldrick, G. M. *SADABS*; University of Göttingen: Göttingen, Germany, 2003.
(46) Sheldrick, G. M. *Acta Crystallogr.* **1990**, *A46*, 467–473.
(47) Sheldrick, G. M. *Acta Crystallogr.* **2008**, *A64*, 112–122.
(48) The program package JulX was used for spin-Hamiltonian simulations and fittings of the data by a full-matrix diagonalization approach (E. Bill, unpublished results).
(49) Glaser, T.; Heidemeier, M.; Krickemeyer, E.; Höke, V. Unpublished results.

complexes $[\{(talen^{t\text{-}Bu_2})Mn_3\}_2\{M(CN)_6\}]^{3+}$.[22,43,49] Besides vibrations of possible counterions, the CN stretching vibrations have been very helpful in probing the formation, purity, and homogeneity of the heptanuclear complexes $[\{(talen^{t\text{-}Bu_2})M'_3\}_2\{M^c(CN)_6\}]^{3+}$. A shift of the CN stretching vibration from 2131 cm^{-1} in the starting complex $[Cr(CN)_6]^{3-}$ to 2153 cm^{-1} accompanied the successful formation of $[\mathbf{Mn_6Cr}]^{3+}$.[22] In the case of the tetranuclear complex $[\mathbf{Mn_3Cr}]^{3+}$, the already weak CN stretching vibration of $[(Me_3tacn)Cr(CN)_3]$[44] at 2133 cm^{-1} becomes even weaker and is barely detectable. Thus, the nondetection of a shifted CN stretching vibration hindered the easy identification of the successful synthesis of $[\mathbf{Mn_3Cr}]^{3+}$.

A comparison of the FTIR spectra of **1** and $[\mathbf{Mn_6Cr}](ClO_4)_3$[50] show the close to 1:1 equivalence of the spectra. The most obvious difference is the relative increase of the ClO_4^- vibrations around 1100 cm^{-1} and at 623 cm^{-1} in **1** due to the higher relative ClO_4^- content: three ClO_4^- per $(talen^{t\text{-}Bu_2})^{6-}$ in **1** versus three ClO_4^- per two $(talen^{t\text{-}Bu_2})^{6-}$ in $[\mathbf{Mn_6Cr}](ClO_4)_3$.[50] The other striking difference is the ν(C≡N) band of medium intensity in $[\mathbf{Mn_6Cr}](ClO_4)_3$ at 2155 cm^{-1}, which is only barely detectable at 2153 cm^{-1} in **1**. However, three weak but well-resolved and reproducible peaks at 1003, 978, and 797 cm^{-1} prove the presence of the $[(Me_3tacn)Cr(CN)_3]$ unit (bands at 1001, 980, and 797 cm^{-1}). These fingerprints will be of value for the identification of other members of the series $[\mathbf{M^t_3M^c}]^{n+}$.

Electrospray ionization mass spectrometry (ESI-MS) of **1** in a CH_3CN/MeOH mixture displays a prominent ion at m/z 523.9 with mass and isotope distribution patterns corresponding to $[\{(talen^{t\text{-}Bu_2})Mn_3\}_2\{(Me_3tacn)Cr(CN)_3\}]^{3+}$. The coordinated methanol molecules do not show up in the MS, indicating the weakness of the $Mn-O^{MeOH}$ bond. The weakness of this sixth coordination site of Mn^{III} was also found in other Mn^{III} triplesalen complexes.[22,24,43]

The electronic absorption spectrum of **1** dissolved in MeOH exhibits very intense transitions in the region above 20 000 cm^{-1} (Figure 1a) and a small absorption at 17 100 cm^{-1} assigned to a d−d transition. The $[(Me_3tacn)Cr(CN)_3]$ building block[44] exhibits only weak d−d bands at 23 300 cm^{-1} (ε = 40 M^{-1} cm^{-1}) and 29 200 cm^{-1} (ε = 65 M^{-1} cm^{-1}) and a more intense feature above 36 000 cm^{-1} (Figure 1a). Thus, this building block gives only negligible contributions to the spectrum of **1**, and the intense features should be assigned to the $[(talen^{t\text{-}Bu_2})Mn_3]^{3+}$ unit of **1**. The black line in Figure 1a corresponds to the spectrum of the building block $[(talen^{t\text{-}Bu_2})\{Mn^{III}(solv)_n\}_3]^{3+}$, as generated in situ in MeOH. The close similarity to the spectrum of **1** dissolved in MeOH raises the question of whether **1** is the main species in methanolic solution. The comparison to the spectrum of $[\mathbf{Mn_6Cr}](ClO_4)_3$[50] in MeOH (red line in Figure 1a) indicates that coordination of $[\mathbf{Mn_3Cr}]^{3+}$ with three facially oriented cyanide groups results in significant distortions of the Mn_3 chromophore. Thus, **1** seems to dissociate into its two building blocks upon dissolution in MeOH.

(50) Höke, V.; Theil, H.; Heidemeier, M.; Weyhermüller, T.; Stammler, A.; Krickemeyer, E.; Bögge, H.; Glaser, T. Manuscript in preparation.

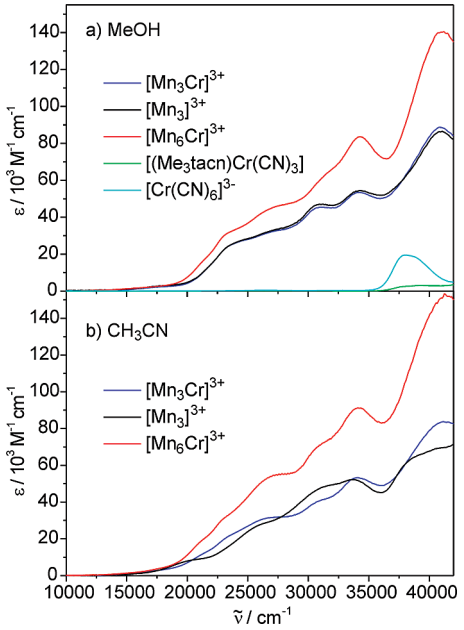

Figure 1. (a) Electronic absorption spectra of **1**, $[(talen^{t\text{-}Bu_2})\{Mn^{III}(solv)_n\}_3]^{3+}$ generated in situ, $[\mathbf{Mn_6Cr}](ClO_4)_3$,[50] $[(Me_3tacn)Cr(CN)_3]$,[44] and $K_3[Cr(CN)_6]$ in MeOH at ambient temperature. (b) Electronic absorption spectra of **1**, $[(talen^{t\text{-}Bu_2})\{Mn^{III}(solv)_n\}_3]^{3+}$ generated in situ, and $[\mathbf{Mn_6Cr}](ClO_4)_3$[50] in CH_3CN at ambient temperature.

We therefore repeated the measurements in a CH_3CN solution (Figure 1b). Interestingly, the spectra of **1** and of the building block $[(talen^{t\text{-}Bu_2})\{Mn^{III}(solv)_n\}_3]^{3+}$ generated in situ in CH_3CN differ. On the other hand, the spectra of **1** and $[\mathbf{Mn_6Cr}](ClO_4)_3$[50] exhibit the same features, albeit with a difference of a factor of roughly 2 in the intensity. Thus, **1** seems to be stable against dissociation into its two building blocks in a CH_3CN solution.

3.2. Structural Characterization. The complex $[\{(talen^{t\text{-}Bu_2})(Mn^{III}(MeOH))_2(Mn^{III}(OAc))\}\{(Me_3tacn)Cr(CN)_3\}](ClO_4)_2\cdot 5MeOH$ (**2**·5MeOH) crystallizes in the space group $P\bar{1}$. The asymmetric unit consists of one formula unit, such that the complex possesses no crystallographically imposed symmetry. The molecular structure of the dication $[\{(talen^{t\text{-}Bu_2})(Mn^{III}(MeOH))_2(Mn^{III}(OAc))\}\{(Me_3tacn)Cr(CN)_3\}]^{2+}$ and the numbering scheme used are illustrated in two orientations in Figure 2. The facial $(N\equiv C)_3$ donor set of $[(Me_3tacn)Cr(CN)_3]$ is coordinated as expected to the three manganese ions of the $[(talen^{t\text{-}Bu_2})Mn_3]^{3+}$ unit. Plots with thermal ellipsoids are provided in different orientations in Figure S1 (Supporting Information), and selected interatomic distances and angles are summarized in Table 1.

The Cr^{III} ion is six-coordinate in a distorted octahedral fashion with Cr−N distances in the range 2.10−2.11 Å and Cr−C distances in the range 2.05−2.07 Å. The N−Cr−N angles of ~84° are smaller than the 90° angle of a regular octahedron due to the steric strain imposed by the macrocyclic ligand Me_3tacn. Two C−Cr−C angles are close to 90°, while the angle C42−Cr−C41 of ~87° is significantly reduced.

The Mn^{III} ions are in an axially elongated octahedral environment. Each Mn^{III} ion is coordinated by two imine nitrogen atoms and two phenolate oxygen atoms of a

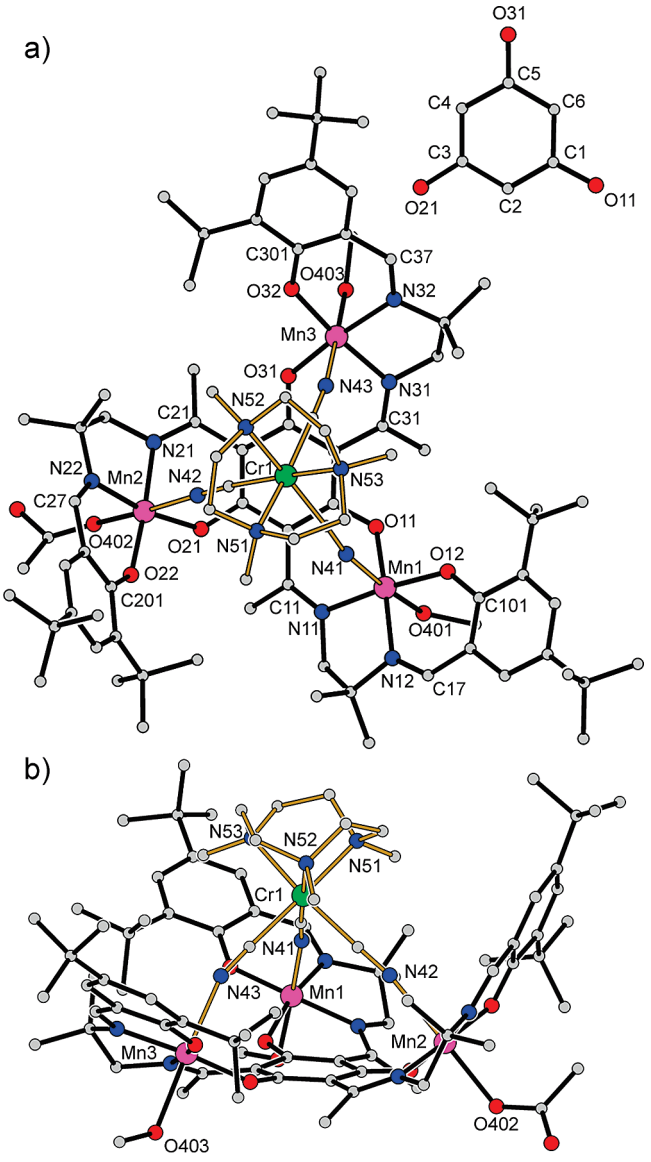

Figure 2. Molecular structure of the dication $[\{(talen^{t\text{-}Bu_2})(Mn^{III}(MeOH))_2(Mn^{III}(OAc))\}\{(Me_3tacn)Cr(CN)_3\}]^{2+}$ in crystals of **2**·5MeOH oriented parallel (a) and perpendicular (b) to the approximate molecular C_3 axis. The bonds of the $[(talen^{t\text{-}Bu_2})(Mn^{III}(MeOH))_2(Mn^{III}(OAc))]^{2+}$ building block are drawn in black, while those of the $[(Me_3tacn)Cr(CN)_3]$ building block are drawn in light brown to guide the eyes. The inset in a provides the numbering scheme for the central phloroglucin unit.

salen-like ligand compartment. The mean values of the Mn−O bond distances for the central PhO^- and the terminal PhO^- are 1.89 and 1.87 Å, respectively, while the mean Mn−N bond distances are 1.97 and 1.98 Å for the central and the terminal imine donors, respectively. The Mn^{III} Jahn−Teller axes are along the $N^{C\equiv N}\cdots O^{MeOH/OAc}$ directions evidenced by longer mean $Mn-N^{N\equiv C}$ and $Mn-O^{MeOH/OAc}$ bond distances of 2.31 and 2.29 Å, respectively.

The sixth coordination sites are occupied by a methanol molecule for Mn1 and Mn3 and by an acetate anion for Mn2. The acetate has a shorter $Mn-O^{OAc}$ distance of 2.206(2) Å in comparison to the $Mn-O^{MeOH}$ distances of 2.337(2) and 2.333(2) Å. These differences do not correlate with the $Mn-N^{N\equiv C}$ bond distance differences in the

Table 1. Selected Interatomic distances [Å] and angles [deg] for **2**·5MeOH

Mn(1)−O(12)	1.876(2)
Mn(1)−O(11)	1.8823(19)
Mn(1)−N(12)	1.976(2)
Mn(1)−N(11)	1.983(2)
Mn(1)−N(41)	2.275(3)
Mn(1)−O(401)	2.337(2)
Mn(2)−O(22)	1.8748(19)
Mn(2)−O(21)	1.8926(19)
Mn(2)−N(21)	1.968(2)
Mn(2)−N(22)	1.981(2)
Mn(2)−O(402)	2.206(2)
Mn(2)−N(42)	2.334(3)
Mn(3)−O(32)	1.867(2)
Mn(3)−O(31)	1.8888(19)
Mn(3)−N(31)	1.968(2)
Mn(3)−N(32)	1.982(2)
Mn(3)−N(43)	2.315(3)
Mn(3)−O(403)	2.333(2)
Cr(1)−C(42)	2.053(3)
Cr(1)−C(43)	2.071(3)
Cr(1)−C(41)	2.074(3)
Cr(1)−N(53)	2.101(3)
Cr(1)−N(51)	2.105(3)
Cr(1)−N(52)	2.109(3)
O(11)−C(1)	1.313(3)
O(12)−C(101)	1.328(3)
O(21)−C(3)	1.312(3)
O(22)−C(201)	1.316(3)
O(31)−C(5)	1.305(3)
O(32)−C(301)	1.323(3)
O(401)−C(401)	1.422(5)
O(402)−C(402)	1.273(4)
O(42A)−C(402)	1.332(7)
O(42B)−C(402)	1.261(9)
O(403)−C(403)	1.434(4)
N(11)−C(11)	1.309(4)
N(12)−C(17)	1.293(4)
N(21)−C(21)	1.302(4)
N(22)−C(27)	1.291(4)
N(31)−C(31)	1.297(4)
N(32)−C(37)	1.287(4)
N(41)−C(41)	1.152(4)
N(42)−C(42)	1.146(4)
N(43)−C(43)	1.147(4)
C(1)−C(2)	1.418(4)
C(1)−C(6)	1.420(4)
C(2)−C(3)	1.430(4)
C(3)−C(4)	1.424(4)
C(4)−C(5)	1.434(4)
C(5)−C(6)	1.424(4)
Mn(1)···Mn(2)	6.7902(6)
Mn(2)···Mn(3)	6.9818(6)
Mn(1)···Mn(3)	6.8674(6)
Mn(1)···Cr(1)	5.4187(6)
Mn(2)···Cr(1)	5.5092(6)
Mn(3)···Cr(1)	5.4392(6)
O(12)−Mn(1)−O(11)	95.89(8)
O(12)−Mn(1)−N(12)	91.20(9)
O(11)−Mn(1)−N(12)	167.54(9)
O(12)−Mn(1)−N(11)	173.87(9)
O(11)−Mn(1)−N(11)	88.76(9)
N(12)−Mn(1)−N(11)	83.53(10)
O(12)−Mn(1)−N(41)	90.62(9)
O(11)−Mn(1)−N(41)	88.72(9)
N(12)−Mn(1)−N(41)	101.47(10)
N(11)−Mn(1)−N(41)	93.48(10)
O(12)−Mn(1)−O(401)	90.12(9)
O(11)−Mn(1)−O(401)	84.56(8)
N(12)−Mn(1)−O(401)	85.19(9)
N(11)−Mn(1)−O(401)	86.34(9)
N(41)−Mn(1)−O(401)	173.28(9)
O(22)−Mn(2)−O(21)	97.25(8)
O(22)−Mn(2)−N(21)	174.05(9)
O(21)−Mn(2)−N(21)	88.48(9)
O(22)−Mn(2)−N(22)	91.60(9)

Table 1. Continued

O(21)−Mn(2)−N(22)	169.19(9)
N(21)−Mn(2)−N(22)	82.53(9)
O(22)−Mn(2)−O(402)	91.60(8)
O(21)−Mn(2)−O(402)	92.18(8)
N(21)−Mn(2)−O(402)	89.78(9)
N(22)−Mn(2)−O(402)	93.76(9)
O(22)−Mn(2)−N(42)	90.06(9)
O(21)−Mn(2)−N(42)	88.29(8)
N(21)−Mn(2)−N(42)	88.50(9)
N(22)−Mn(2)−N(42)	85.50(9)
O(402)−Mn(2)−N(42)	178.20(9)
O(32)−Mn(3)−O(31)	95.17(8)
O(32)−Mn(3)−N(31)	174.24(9)
O(31)−Mn(3)−N(31)	89.70(9)
O(32)−Mn(3)−N(32)	92.00(9)
O(31)−Mn(3)−N(32)	171.97(10)
N(31)−Mn(3)−N(32)	82.95(10)
O(32)−Mn(3)−N(43)	92.41(10)
O(31)−Mn(3)−N(43)	88.44(9)
N(31)−Mn(3)−N(43)	90.79(10)
N(32)−Mn(3)−N(43)	94.87(10)
O(32)−Mn(3)−O(403)	88.20(9)
O(31)−Mn(3)−O(403)	89.11(8)
N(31)−Mn(3)−O(403)	88.81(10)
N(32)−Mn(3)−O(403)	87.51(9)
N(43)−Mn(3)−O(403)	177.52(9)
C(42)−Cr(1)−C(43)	90.04(11)
C(42)−Cr(1)−C(41)	86.98(12)
C(43)−Cr(1)−C(41)	90.28(12)
C(42)−Cr(1)−N(53)	175.00(11)
C(43)−Cr(1)−N(53)	94.72(11)
C(41)−Cr(1)−N(53)	94.53(11)
C(42)−Cr(1)−N(51)	90.78(11)
C(43)−Cr(1)−N(51)	175.92(12)
C(41)−Cr(1)−N(51)	93.76(11)
N(53)−Cr(1)−N(51)	84.37(11)
C(42)−Cr(1)−N(52)	94.88(11)
C(43)−Cr(1)−N(52)	92.54(11)
C(41)−Cr(1)−N(52)	176.63(11)
N(53)−Cr(1)−N(52)	83.39(10)
N(51)−Cr(1)−N(52)	83.41(11)
C(41)−N(41)−Mn(1)	161.4(2)
C(42)−N(42)−Mn(2)	170.4(2)
C(43)−N(43)−Mn(3)	160.0(2)
N(41)−C(41)−Cr(1)	175.7(3)
N(42)−C(42)−Cr(1)	175.6(3)
N(43)−C(43)−Cr(1)	177.6(3)

trans position. The Mn1−N41 distance of 2.275(3) Å is shorter in comparison to the Mn2−N42 of 2.334(3) Å and the Mn3−N43 of 2.315(3) Å, although N42 coordinated to Mn2 is trans to the acetate.

An important consideration for the Mn−Cr exchange interaction is the geometry of the Mn−N≡C−Cr pathway. Selected mean structural parameters are summarized in Table 2. A nonlinearity is observed in the Mn−N≡C angles, with values of 160.0° and 161.4° for Mn1 and Mn3, respectively, and a significantly larger value of 170.4° for the acetate-coordinated Mn2. This bending is common for the Mn−N≡C−Cr(CN)$_n$ unit. A search in the Cambridge Structural Database provided 53 compounds, where the mean values are 175.0° and 160.4° for the N≡C−Cr angles and the Mn−N≡C angles, respectively. However, the distribution of N≡C−Cr angles is only over a range of 10.3°, while the Mn−N≡C angles are distributed over a wide range of 41.3°, indicating a flat potential for bending of this mode. Thus, the bending of the Mn−N≡C units introduces no significant strain, which would decrease the energetic driving force for the formation of the tetranuclear complexes. The bending does not occur randomly, but rather all three Mn−N≡C units bend toward the approximate molecular C_3 axis. Thus, the tetrahedron built of Cr and the three N atoms of the cyanides is elongated along this axis.

An important aspect for the Mn−Mn exchange interaction is the overall geometry of the trinuclear triplesalen building block. The bent angles $\varphi_{central}$ and $\varphi_{terminal}$ are appropriate parameters to quantitatively describe the ligand folding in the trinuclear triplesalen building blocks.[20,23,24] The bent angle φ[51] is defined by $\varphi = 180° - \angle(M-X_{NO}-X_R)$ (X_{NO}, midpoint of adjacent N and O donor atoms; X_R, midpoint of the six-membered chelate ring containing the N and O donor atoms). This bent angle is best suited to differentiate between a bending along an idealized line through neighboring N and O ligands and a line perpendicular to the former, resulting in a helical distortion.[20] In the trinuclear Ni^{II} and Cu^{II} complexes, $\varphi_{central}$ is in the range 20−30° while $\varphi_{terminal}$ is significantly smaller in the range 3−9°. Coordination of [(Me$_3$tacn)Cr(CN)$_3$] in **2** results obviously in a greater degree of bending (Table 2). The bent angles in **2** differ significantly for Mn1 and Mn3 ($\varphi_{central}$ = 34.4°, 32.0°; $\varphi_{terminal}$ = 10.4°, 9.4°) on the one hand and for the acetate-coordinated Mn2 ($\varphi_{central}$ = 41.1°; $\varphi_{terminal}$ = 27.5°) on the other hand.

Complex **1** crystallizes with two independent molecules of [(talen$^{t\text{-}Bu_2}$)(Mn^{III}(MeOH))$_3$]$^{3+}$ in the unit cell (Figure S2, Supporting Information). As the diffraction data do not allow the refinement of the network of uncoordinated solvent, we refrain from a detailed discussion on the molecular and crystal structure. However, the two cations [**Mn$^{III}_3$Cr^{III}**]$^{3+}$ are well-defined so that the overall geometries and mean structural parameters can be compared to those of [**Mn$^{III}_3$Cr^{III}**]$^{3+}$ in **2**·5MeOH. The two [**Mn$^{III}_3$Cr^{III}**]$^{3+}$ complexes in **1** have the same overall structure as that of **2** despite having no acetate but MeOH coordinated to the Mn^{III} ions. The Mn−O and Mn−N distances to the triplesalen ligand are not distinguishable from that of **2**. The mean structural parameters relevant for the exchange pathways are summarized in Table 2.

3.3. Magnetic Measurements. Temperature-dependent dc magnetic susceptibility measurements (2−290 K, 1 T) on powdered samples of **1** reveal μ_{eff} = 9.20 μ_B at 290 K, which decreases monotonically with decreasing temperature to a minimum of 4.13 μ_B at 2 K (Figure 3a). The room-temperature value is close to the spin-only value (g_i = 2.00) for an uncoupled system of three high-spin Mn^{III} (S_i = 2) and one Cr^{III} (S_i = 3/2) of 9.33 μ_B.

The continuous decrease of μ_{eff} indicates dominating antiferromagnetic interactions between the metal ions. However, antiferromagnetic interactions between the central Cr^{III} ion and the Mn^{III} ions should result in an increase of μ_{eff} at lower temperatures due to a ferrimagnetic coupling scheme, as was observed in [**Mn$^{III}_6$Cr^{III}**]$^{3+}$.[22] Therefore, the continuous decrease of μ_{eff} with decreasing temperature might indicate that the antiferromagnetic interaction of $J_{Mn-Cr} = -5.0$ cm^{-1} in [**Mn$^{III}_6$Cr^{III}**]$^{3+}$[22] is weakened in **1**.

VTVH magnetization measurements for **1** at several magnetic fields exhibit a strong nesting of the isofield lines

(51) Cavallo, L.; Jacobsen, H. *Eur. J. Inorg. Chem.* **2003**, 892–902.

Table 2. Collection of J_{Mn-Cr} Exchange Coupling Constants and Structural Parameters (Mean Values) of the Mn−N≡C−Cr Exchange Pathway for Salen-Mn^{III} Fragments Bridged by a $[Cr^{III}(CN)]^{3-}$ or $[(Me_3tacn)Cr^{III}(CN)]$

	J_{Mn-Cr}/ cm^{-1}	d(Mn−$N^{N\equiv C}$)/Å	∠(Mn−N≡C)	∠(N≡C−Cr)	d(Cr−$C^{C\equiv N}$)/Å	d(N≡C)/Å	J_{Mn-Mn}/ cm^{-1}	$\varphi_{central}$	ref.
$[Mn^{III}_3Cr^{III}]^{3+}$ in **2**·5MeOH		2.31	163.9°	176.3°	2.07	1.15		33.2	this work
$[Mn^{III}_3Cr^{III}]^{3+}$ in **1**	−0.12	2.29	163.6°	176.2°	2.07	1.15	−0.7	35.8	this work
$[Mn^{III}_6Cr^{III}]^{3+}$	−5.0	2.18	161.3°	176.1°	2.07	1.15	−1.0	46.7	22
$[\{(salen)Mn^{III}(OH_2)\}_6\{Cr^{III}(CN)_6\}]^{3+}$ (**A**)	−2.5	2.32	149.9°	176.6°	2.08	1.15			64, 65
$[\{(5\text{-Brsalen})Mn^{III}(OH_2)\}_2\{Cr^{III}(CN)_6\}]^{-}$ (**B**)	−6.3	2.34	141.9°	176.9°	2.08	1.16			40
$[\{(salen)Mn^{III}(EtOH)\}_3\{Cr^{III}(CN)_6\}]$ (**C**)	−1.6	2.27	160.1°	174.8°	2.08	1.16			58
mean values from 53 compounds and 89 fragments		2.23	160.4°	175.0°	2.07	1.14			CSD search [a]

[a] Note that the formal oxidation states of the Mn and Cr ions in the CSD search are not necessarily +III.

(Figure 3b). This behavior is commonly attributed to a strong magnetic anisotropy,[52] but the nesting is more generally an indication that the energy differences between the lowest $|m_S\rangle$ levels are on the order of the Zeeman energy so that the identities of the ground $|m_S\rangle$ levels are field- and orientation-dependent. The energy splitting of the lowest $|m_S\rangle$ levels can either arise from zero-field splitting or weak exchange couplings.

In order to obtain some quantitative insight into the magnitudes and ratios of the exchange coupling constants J_{ij} and the axial zero-field splitting parameters D_i, we have performed a full-matrix diagonalization of the appropriate spin-Hamiltonian (eq 1) including isotropic HDvV exchange, zero-field splitting, and Zeeman interaction.[48]

$$\begin{aligned}\check{H} = & -2J_{Mn-Cr}(\mathbf{S}_1\mathbf{S}_4 + \mathbf{S}_2\mathbf{S}_4 \\ & + \mathbf{S}_3\mathbf{S}_4) - 2J_{Mn-Mn}(\mathbf{S}_1\mathbf{S}_2 + \mathbf{S}_2\mathbf{S}_3 + \mathbf{S}_3\mathbf{S}_1) \\ & + \sum_{i=1}^{3}\{D_{Mn}[S^2_{z,i} - 1/3S_i(S_i+1)]\} \\ & + D_{Cr}[S^2_{z,4} - 1/3S_4(S_4+1)] \\ & + \mu_B\sum_{i=1}^{3}(g_{Mn}\mathbf{S}_i\mathbf{B}) + \mu_B g_{Cr}\mathbf{S}_4\mathbf{B} \qquad (1)\end{aligned}$$

The topology of $[\mathbf{Mn^{III}_3Cr^{III}}]^{3+}$ requires a coupling scheme with two different coupling constants: J_{Mn-Cr} describes the interaction between each Mn^{III} ($\mathbf{S_1}$ to $\mathbf{S_3}$) with the Cr^{III} ($\mathbf{S_4}$), and J_{Mn-Mn} describes the interaction between pairs of Mn^{III} ions in the trinuclear triplesalen building block. The second line corresponds to the local zero-field splittings and the third line to the local Zeeman interactions.

We started the procedure by simulating the data for the values of $J_{Mn-Cr} = -5.0\ cm^{-1}$ and $J_{Mn-Mn} = -1.0\ cm^{-1}$ obtained for $[\mathbf{Mn^{III}_6Cr^{III}}]^{3+}$[22] with $D_{Mn} = -3.0\ cm^{-1}$ obtained for $[\mathbf{Mn^{III}_6Fe^{III}}]^{3+}$.[43] As expected (vide supra), the calculated μ_{eff} versus T curve (red curve in Figure 4a) decreases from room temperature to a minimum around 35 K and increases on further cooling to a value of 8.51 μ_B at 5 K. Additionally, the corresponding simulated VTVH data (not shown) exhibit a lower saturation magnetization at 7 T and a smaller nesting behavior of the isofield lines. Reasonable reproductions of the experimental values required a strong decrease of J_{Mn-Cr} and also a decrease of J_{Mn-Mn}.

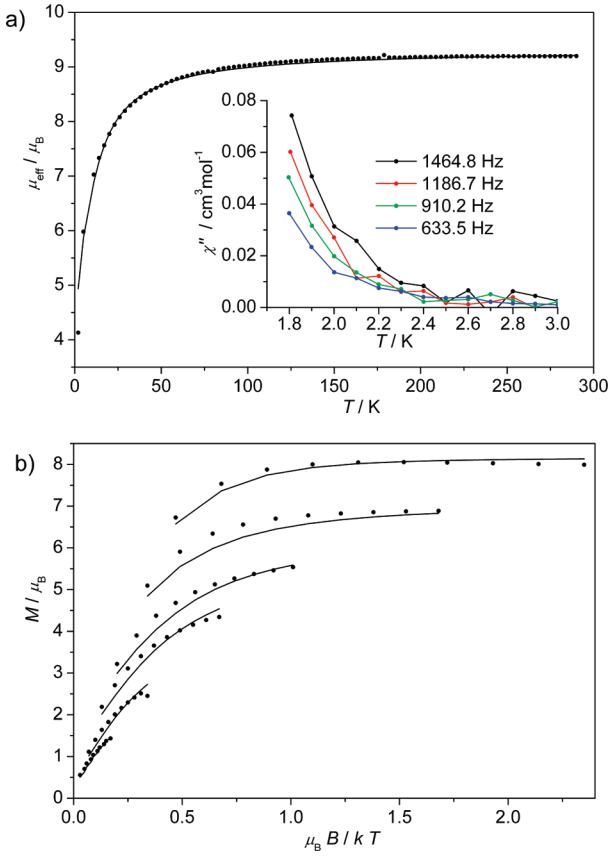

Figure 3. (a) Temperature dependence of μ_{eff} at 1 T of **1**. Inset: Temperature and frequency dependence of χ'' in an oscillating 3 Oe ac field and a zero dc field. (b) VTVH magnetization measurements at 0.5, 1, 2, 3, 5, and 7 T for **1**. Experimental data are given as circles. The solid lines in both figures correspond to the best simulation based on the complete spin-Hamiltonian by full-matrix diagonalization using $J_{Mn-Cr} = -0.700\ cm^{-1}$, $J_{Mn-Mn} = -0.123\ cm^{-1}$, $D_{Mn} = -3.00\ cm^{-1}$, $D_{Cr} = 0$, and $g_{Mn} = g_{Cr} = 2.00$.

Figure 4a shows variations of J_{Mn-Cr} for $J_{Mn-Mn} = -1.00\ cm^{-1}$ and $D_{Mn} = -3.0\ cm^{-1}$ fixed. It is quite evident that, for the chosen parameters of J_{Mn-Mn} and D_{Mn}, J_{Mn-Cr} should be in the range −1 to 0 cm^{-1}. Figure 4b shows the variation of J_{Mn-Mn} for $J_{Mn-Cr} = -0.1\ cm^{-1}$ and $D_{Mn} = -3.0\ cm^{-1}$ fixed. For the chosen parameters of J_{Mn-Cr} and D_{Mn}, $J_{Mn-Mn} = -0.7\ cm^{-1}$ seems quite reasonable. In order to obtain the best values, we investigated two-dimensional contour projections of

(52) Girerd, J.-J.; Journaux, Y. In *Physical Methods in Bioinorganic Chemistry*; Que, L. J., Ed.; University Science Books: Sausalito, CA, 2000; pp 321−374.

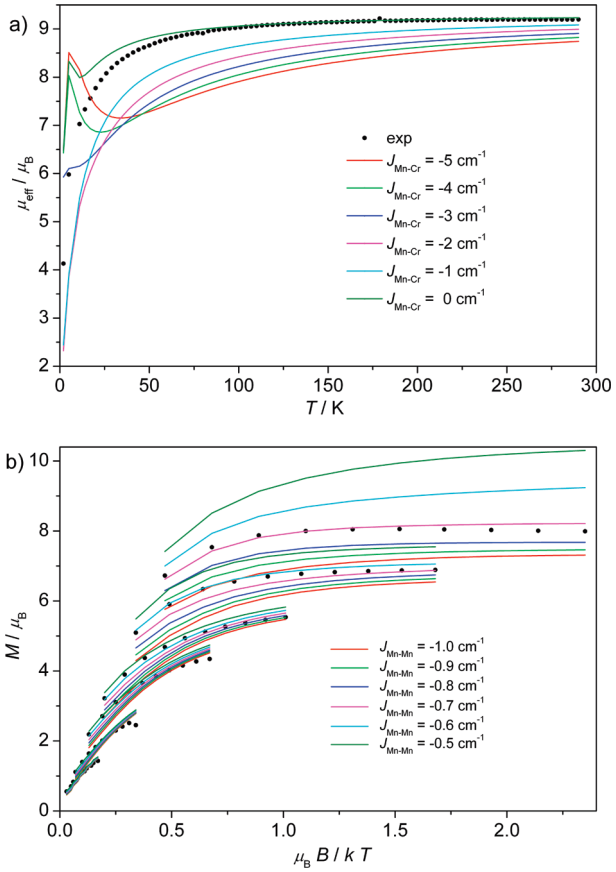

Figure 4. (a) Temperature dependence of μ_{eff} at 1 T of **1**. Experimental data given as circles. The lines correspond to simulations based on the complete spin-Hamiltonian by full-matrix diagonalization. The simulations are performed with variation of J_{Mn-Cr} and fixed parameters $J_{Mn-Mn} = -1.00$ cm^{-1}, $D_{Mn} = -3.00$ cm^{-1}, $D_{Cr} = 0$, and $g_{Mn} = g_{Cr} = 2.00$. (b) VTVH magnetization measurements at 0.5, 1, 2, 3, 5, and 7 T for **1**. Experimental data given as circles. The lines correspond to simulations based on the complete spin-Hamiltonian by full-matrix diagonalitzation. The simulations are performed with variation of J_{Mn-Mn} and fixed parameters $J_{Mn-Cr} = -0.10$ cm^{-1}, $D_{Mn} = -3.00$ cm^{-1}, $D_{Cr} = 0$, and $g_{Mn} = g_{Cr} = 2.00$.

relative error surfaces for varying J_{Mn-Cr} and J_{Mn-Mn} using fixed values of the other parameters and performed several fitting procedures. It became evident that the magnitude of D_{Mn} must be around -3 cm^{-1} and that the incorporation of a D_{Cr} of $+1$ cm^{-1} or -1 cm^{-1} has no significant effect. By using these combined strategies, a reasonable range of parameters that reproduce both the temperature-dependent magnetization and the VTVH magnetization data is $J_{Mn-Cr} = -0.12 \pm 0.04$ cm^{-1}, $J_{Mn-Mn} = -0.70 \pm 0.03$ cm^{-1}, $D_{Mn} = -3.0 \pm 0.4$ cm^{-1} with $g_{Cr} = g_{Mn} = 2.00$, and $D_{Cr} = 0$ cm^{-1} (see solid lines in Figure 3a and b).

Figure 5 shows the field-dependence of the lowest $|m_S\rangle$ levels calculated using the best parameters given above for the z direction (Figure 5a) and the x direction (Figure 5b, equivalent to the y direction due to the symmetry of the spin-Hamiltonian, eq 1). Despite the relatively low J values, a spin-manifold composed of $|m_S = \pm 1/2\rangle$, $|m_S = \pm 3/2\rangle$, $|m_S = \pm 5/2\rangle$, and $|m_S = \pm 7/2\rangle$ Kramers doublets is energetically separated from the other levels by $\sim$6 cm^{-1}. Each $|m_S\rangle$ state is three-fold degenerate. These pseudo $S_t = 7/2$ total spin states are split in the zero field by $\sim$1.5 cm^{-1}, and the $|\pm 1/2\rangle$

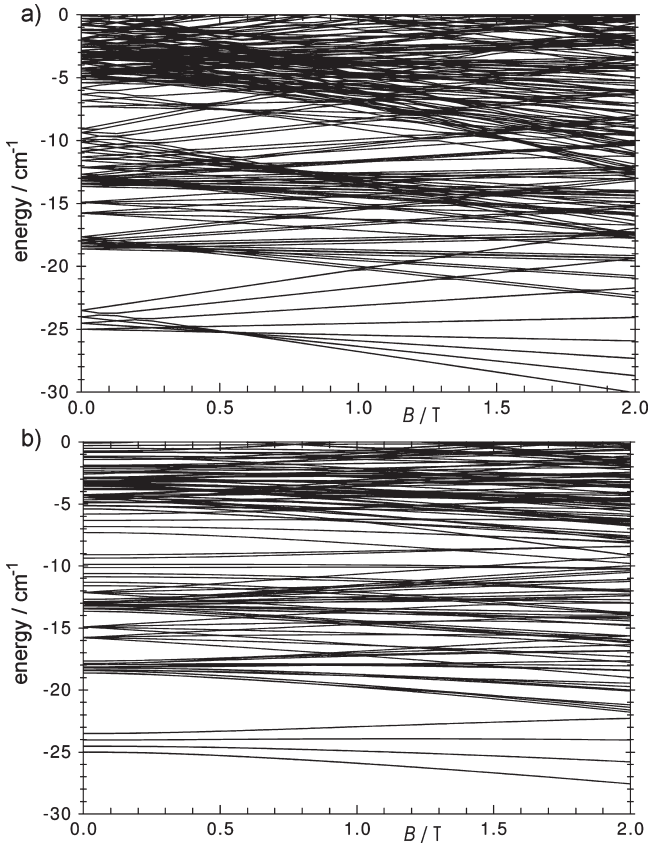

Figure 5. Field dependence of the eigenfunctions of the spin-Hamiltonian (**1**) by full-matrix diagonalization using $J_{Mn-Cr} = -0.700$ cm^{-1}, $J_{Mn-Mn} = -0.123$ cm^{-1}, $D_{Mn} = -3.00$ cm^{-1}, $D_{Cr} = 0$, and $g_{Mn} = g_{Cr} = 2.00$. (a) z direction; (b) x direction.

Kramers doublet as a ground state implies a positive zero-field dependence.

It is interesting to analyze the field dependence of these lowest $|m_S\rangle$ levels. In the x and y directions and thus in the whole $x-y$ plane, a weak field dependence and consequently a weak magnetization are found, while the field dependence of the Kramers doublets is stronger in the z direction. This leads to the surprising conclusion that the magnetization of this system is better described as an easy-axis system rather than an easy-plane system despite the apparent positive value of $D_{St=7/2}$.

It is important to emphasize that the zero-field splitting terms, the HDvV terms, and the Zeeman terms of the full spin-Hamiltonian, eq 1, are all on the same order of magnitude. This leads to a complex field- and orientation-dependent mixing of $|m_S\rangle$ wave functions. The field-dependent mixing is easily visible in the curved nature of the eigenfunctions in the y direction (Figure 5b).

The three degenerate $|m_S = -1/2\rangle$ eigenfunctions are mainly linear combinations of the following three basis function written as $|m_{s1},m_{s2},m_{s3},m_{s4}\rangle$: $|-2,-2,+2,+3/2\rangle$, $|-2,+2,-2,+3/2\rangle$, and $|+2,-2,-2,+3/2\rangle$, whereas the three degenerate $|m_S = +1/2\rangle$ eigenfunctions are correspondingly mainly composed of $|-2,+2,+2,-3/2\rangle$, $|+2,-2,+2,-3/2\rangle$, and $|+2,+2,-2,-3/2\rangle$. The three-fold degeneracy of the energy levels is a consequence of the three-fold symmetry of the system and a manifestation of the spin-frustration in the trinuclear Mn^{III}_3 triple-salen unit with antiferromagnetic J_{Mn-Mn} interactions.

It must be emphasized that the three-fold degenerate $|m_S = \pm 1/2\rangle$, $|m_S = \pm 3/2\rangle$, $|m_S = \pm 5/2\rangle$, and $|m_S = \pm 7/2\rangle$ Kramers doublets are not components of three "good" $S_t = 7/2$ spin ground states, with S_t being a good quantum number. The energies of the Kramers doublets for a "good" $S_t = 7/2$ system are not equidistant but rather lie at energies of 0, $2D$, $6D$, and $12D$ for $|m_S = \pm 1/2\rangle$, $|m_S = \pm 3/2\rangle$, $|m_S = \pm 5/2\rangle$, and $|m_S = \pm 7/2\rangle$, respectively. Thus, the simple approximation by using the spin-Hamiltonian for only one spin ground state S_t (effective spin model or giant spin model) cannot adequately describe this field- and orientation-dependent mixing of $|s_1,m_{s1},s_2,m_{s2},s_3,m_{s3},s_4,m_{s4}\rangle$ wave functions.

The weak easy-axis magnetic anisotropy in the slightly stabilized $|m_S\rangle$ states is corroborated by the onset of a frequency-dependent χ'' signal in the ac magnetization measurements (inset in Figure 3a). This is consistent with a slow relaxation of the magnetization and is an indication that **1** is a SMM.

4. Discussion

4.1. Discussion of the Mn−Cr Exchange Pathway. The exchange coupling in the $Mn^{III}-N\equiv C-Cr^{III}$ unit can be analyzed by using heuristic concepts in magnetochemistry.[31,37−39] According to the first and second Goodenough−Kanomori rules,[53−57] this Cr^{III} $(t_{2g}^3)-Mn^{III}$ $(t_{2g}^3e_g^1)$ system would exhibit both antiferromagnetic $(t_{2g}-t_{2g})$ and ferromagnetic pathways $(t_{2g}-e_g)$, respectively. As usual, the antiferromagnetic pathways are stronger in comparison to ferromagnetic pathways. Additional pathways of lower strength arise according to the third Goodenough−Kanamori rule like the ferromagnetic pathway Cr^{III} $(e_g^0)-Mn^{III}$ (e_g^1). However, such an analysis is only valid in the hypothetical limit of regular O_h symmetry for both ions with the $C\equiv N^-$ linker along the z axis and no rotation of the two local xy axes. Real $Mn^{III}-N\equiv C-Cr^{III}$ systems exhibit several degrees of distortion in comparison to the ideal symmetry: bending of the Mn−N≡C angle, rotation of the local xy coordinate systems relative to each other, bending of the equatorial coordination planes with respect to the C≡N vector, and many more.

There have been several reports in the literature on the exchange coupling in the $Mn^{III}-N\equiv C-Cr^{III}$ unit[58,59] and in the corresponding $Mn^{II}-N\equiv C-Cr^{III}$ unit.[60−63] For both, a linear correlation of the coupling constant for the Mn−N≡C−Cr exchange pathway with the angle ∠(Mn−N≡C) has been proposed. The antiferromagnetic coupling increases with decreasing angle, that is, the stronger the bending, the stronger the antiferromagnetic coupling.[59] It should be noted that all magnetic data in the aforementioned publications have been analyzed with an isotropic spin-Hamiltonian including isotropic HDvV exchange but neglecting the zero-field splitting contributions. Thus, the simulations/fittings for the values of J may account for effects of D.

Table 2 summarizes J_{Mn-Cr} and structural parameters for $(salen)Mn^{III}-N\equiv C-Cr(CN)_n$ systems. In comparing the three compounds **A**,[64,65] **B**,[40] and **C**,[58] the almost linear correlation of J_{Mn-Cr} with the angle ∠(Mn−N≡C) is obvious. However, the angles of $[\mathbf{Mn^{III}_3Cr^{III}}]^{3+}$ (163.6°) and $[\mathbf{Mn^{III}_6Cr^{III}}]^{3+}$ (161.7°) are close to the value of 160.1° of compound **C**. Thus, the known magneto-structural correlations regarding the angle ∠(Mn−N≡C) cannot explain the differences in J_{Mn-Cr}. Generally, exchange couplings are stronger for more covalent superexchange pathways,[66] and the covalency increases with decreasing bond distance. The only significant difference is in the $Mn-N^{N\equiv C}$ bond distances, with the mean value of $[\mathbf{Mn^{III}_3Cr^{III}}]^{3+}$ of 2.29 Å being remarkably longer than the value of 2.18 Å for $[\mathbf{Mn^{III}_6Cr^{III}}]^{3+}$. Furthermore, a correlation of J_{Mn-Cr} with $d(Mn-N^{N\equiv C})$ is apparent for $[\mathbf{Mn^{III}_3Cr^{III}}]^{3+}$, $[\mathbf{Mn^{III}_6Cr^{III}}]^{3+}$, and **C**, all having approximately the same angle ∠(Mn−N≡C). Thus, the strong antiferromagnetic interaction in $[\mathbf{Mn^{III}_6Cr^{III}}]^{3+}$ can be ascribed to the short $Mn-N^{N\equiv C}$ bond distance of 2.18 Å, which is a distinctive feature of $[\mathbf{Mn^{III}_6Cr^{III}}]^{3+}$, as the other compounds all exhibit much longer Mn−N distances.

4.2. Discussion on the Mn−Mn Exchange Pathway. The trinuclear Mn^{III} triplesalen building blocks have some degree of freedom to orient the three Mn^{III} ions for optimal bonding to the facially arranged cyanide nitrogen atoms, which result in different orientations of the magnetic d orbitals relative to the phenolate p orbitals. Our studies on the trinuclear triplesalen complexes indicate that variations in these orientations can have a strong impact on the two different mechanisms, spin-polarization and spin-delocalization,[67] and thus on the overall exchange interaction of the three Mn^{III} ions through the phloroglucinol unit.

The measurements of $[\mathbf{Mn^{III}_3Cr^{III}}]^{3+}$ manifest that the exchange coupling through the phloroglucinol bridging unit is antiferromagnetic in nature for Mn^{III} ions, despite the ferromagnetic couplings observed in trinuclear Cu^{II} complexes[18,21,23] and a $V^{IV}{=}O$ complex.[25] A crucial parameter for an efficient spin-polarization mechanism through the bridging benzene unit was found to be the amount of spin-density in the p_z^{π} orbitals of the phenolic oxygen atoms.[67] This spin-density depends on the metal ion, the remaining coordination sites, and the ligand folding at the central metal−phenolate bond, which

(53) Goodenough, J. B. *Magnetism and the Chemical Bond*; Interscience: New York, 1963.
(54) Kanamori, J. *J. Phys. Chem. Solids* **1959**, *10*, 87–98.
(55) Anderson, P. W. *Phys. Rev.* **1959**, *115*, 2–13.
(56) Anderson, P. W. *Magnetism*; Academic Press: New York, 1963.
(57) Weihe, H.; Güdel, H. U. *Inorg. Chem.* **1997**, *36*, 3632–3639.
(58) Miyasaka, H.; Takahashi, H.; Madanbahsi, T.; Sugiura, K.-i.; Clerac, R.; Nojiri, H. *Inorg. Chem.* **2005**, *44*, 5969–5971.
(59) Pan, F.; Wang, Z.-M.; Gao, S. *Inorg. Chem.* **2007**, *46*, 10221–10228.
(60) Toma, L.; Lescouezec, R.; Vaissermann, J.; Delgado, F. S.; Ruiz-Pérez, C.; Carrasco, R.; Cano, J.; Lloret, F.; Julve, M. *Chem.—Eur. J.* **2004**, 6130–6145.
(61) Zhang, Y.-Z.; Gao, S.; Wang, Z.-M.; Su, G.; Sun, H.-L.; Pan, F. *Inorg. Chem.* **2005**, *44*, 4534–4545.
(62) Atanasov, M.; Busche, C.; Comba, P.; Hallak, F. E.; Martin, B.; Rajaraman, G.; van Slageren, J.; Wadepohl, H. *Inorg. Chem.* **2008**, *47*, 8112–8125.
(63) Heinrich, J. L.; Sokol, J. J.; Hee, A. G.; Long, J. R. *J. Solid State Chem.* **2001**, *159*, 293–301.
(64) Shen, X. P.; Li, B. L.; Zou, J. Z.; Xu, Z.; Yu, Y. P.; Liu, S. X. *Trans. Met. Chem.* **2002**, *4*, 372.
(65) Choi, H. J.; Sokol, J. J.; Long, J. R. *J. Phys. Chem. Solids* **2004**, *65*, 839–844.
(66) Glaser, T.; Rose, K.; Shadle, S. E.; Hedman, B.; Hodgson, K. E.; Solomon, E. I. *J. Am. Chem. Soc.* **2001**, *123*, 442–454.
(67) Glaser, T.; Theil, H.; Heidemeier, M. *C. R. Chim.* **2008**, *11*, 1121–1136.

differs strongly for $[\mathbf{Mn^{III}_3Cr^{III}}]^{3+}$ and $[\mathbf{Mn^{III}_6Cr^{III}}]^{3+}$: 35.8° versus 46.7°.

4.3. Origin of the Differences in Driving Force for Formation and in the J_{Mn-Cr} Exchange Coupling between $[\mathbf{Mn^{III}_6Cr^{III}}]^{3+}$ and $[\mathbf{Mn^{III}_3Cr^{III}}]^{3+}$. It seems evident that the high driving force for formation, the short $Mn-N^{N\equiv C}$ bond distance and therefore the value of J_{Mn-Cr}, are special for $[\mathbf{Mn^{III}_6Cr^{III}}]^{3+}$. It is therefore interesting to speculate whether there is a common origin for this and what it may be.

The Mn^{III} ions in $[\mathbf{Mn^{III}_3Cr^{III}}]^{3+}$ and $[\mathbf{Mn^{III}_6Cr^{III}}]^{3+}$ are coordinated by the same triplesalen ligand $(talen^{t\text{-}Bu_2})^{6-}$. As the preorganization of the building block $[(talen^{t\text{-}Bu_2})\{Mn^{III}(solv)_n\}_3]^{3+}$ is the same in both cases (Scheme 1) and the orientation of the *fac*-$(N\equiv C)_3$ donor sets of $[Cr(CN)_6]^{3-}$ and of $[(Me_3tacn)Cr(CN)_3]$ is the same, additional contributions to the driving force for the formation of $[\mathbf{Mn^{III}_6Cr^{III}}]^{3+}$ must be present, which are absent in the formation of $[\mathbf{Mn^{III}_3Cr^{III}}]^{3+}$.

The only clear difference in the formation process of $[\mathbf{Mn^{III}_6Cr^{III}}]^{3+}$ and $[\mathbf{Mn^{III}_3Cr^{III}}]^{3+}$ is the overall charge of the *fac*-$(N\equiv C)_3$ donor sets: whereas $[Cr(CN)_6]^{3-}$ is a trianion, $[(Me_3tacn)Cr(CN)_3]$ is a neutral molecule. As the building block $[(talen^{t\text{-}Bu_2})\{Mn^{III}(solv)_n\}_3]^{3+}$, which is common for both processes, is a trication, there are electrostatic attractions between the building blocks involved in the formation of $[\mathbf{Mn^{III}_6Cr^{III}}]^{3+}$, which are absent in the formation of $[\mathbf{Mn^{III}_3Cr^{III}}]^{3+}$. Thus, the high driving force for the formation of $[\mathbf{Mn^{III}_6Cr^{III}}]^{3+}$ should include some attractive electrostatic forces in addition to the molecular recognition.

The high driving force for the $[\mathbf{Mn^{III}_6Cr^{III}}]^{3+}$ formation is correlated with the short $Mn-N^{N\equiv C}$ bond length. It may be argued that the electrostatic attraction leads to the shorter bond distance, therefore to the higher $Mn-N^{N\equiv C}$ bond strength, and thus the higher driving force. However, a close inspection of Table 2 shows that the three compounds **B**,[40] **C**,[58] and especially the closely related species $[\{(salen)Mn^{III}(OH_2)\}_6\{Cr^{III}(CN)_6\}]^{3+}$ (**A**),[64,65] which all possess the $[Cr(CN)_6]^{3-}$ building block, feature the longer $Mn-N^{N\equiv C}$ bond distances. Thus, differences in electrostatic attraction might be the source of some part of the differences between $[\mathbf{Mn^{III}_3Cr^{III}}]^{3+}$ and $[\mathbf{Mn^{III}_6Cr^{III}}]^{3+}$, but they cannot be the single source for the short $Mn-N^{N\equiv C}$ bond length in $[\mathbf{Mn^{III}_6Cr^{III}}]^{3+}$.

An important aspect for the origin of the short $Mn-N^{N\equiv C}$ bond arises from a consideration of the ligand folding. The terminal bending is comparable for $[\mathbf{Mn^{III}_3Cr^{III}}]^{3+}$ (16.7°) and $[\mathbf{Mn^{III}_6Cr^{III}}]^{3+}$ (15.8°), while the mean bending at the central phenolates is strongly reduced in $[\mathbf{Mn^{III}_3Cr^{III}}]^{3+}$ (35.8° vs 46.7° in $[\mathbf{Mn^{III}_6Cr^{III}}]^{3+}$). There may be two reasons for stronger ligand folding in $[\mathbf{Mn^{III}_6Cr^{III}}]^{3+}$. The shorter $Mn^{III}-N^{N\equiv C}$ bond distances force the Mn^{III} ions to come closer together in order to be better oriented for the orbital overlap with the $N^{N\equiv C}$ atoms. Additionally, there seems to be some driving force for the dimerization of two $[(talen^{t\text{-}Bu_2})\{M(solv)_n\}_3]^{m+}$ units. For example, two bowl-shaped $[(talen^{t\text{-}Bu_2})Cu^{II}_3]$ complexes can encapsulate two CH_2Cl_2 molecules,[23] or two $[(talen^{t\text{-}Bu_2})\{Fe^{III}(MeOH)(H_2O)\}_3]^{3+}$ units can encapsulate the uncommon $[Cl\cdots H\cdots Cl]^-$ unit.[49] A close inspection of the molecular structures of these supramolecular aggregates and of the heptanuclear complexes $[\mathbf{M^t_6M^c}]^{n+}$ (see space-filling model of $[\mathbf{Mn^{III}_6Fe^{III}}]^{3+}$ in ref 43) indicates some kind of van der Waals type contacts between the two trinuclear triplesalen building blocks. In this respect, the absence of a second triplesalen complex in $[\mathbf{Mn^{III}_3Cr^{III}}]^{3+}$ may reduce the driving force for ligand folding. Therefore, the short $Mn-N^{N\equiv C}$ bond is not the reason for a stronger ligand folding, but the stronger supramolecular attraction between the two $[(talen^{t\text{-}Bu_2})Mn^{III}_3]^{3+}$ subunits in $[\mathbf{Mn^{III}_6Cr^{III}}]^{3+}$ forces a more substantial bending and thus enforces shorter $Mn-N^{N\equiv C}$ bond distances and therefore a higher $Mn-N^{N\equiv C}$ bond strength. This then leads to the observed high driving force for $[\mathbf{Mn^{III}_6M^{III}}]^{3+}$ formation and thus to the strong J_{Mn-Cr} coupling, which is the origin for $[\mathbf{Mn^{III}_6Cr^{III}}]^{3+}$ being a good SMM.

Conclusions

The molecular building block $[(talen^{t\text{-}Bu_2})\{Mn^{III}(solv)_n\}_3]^{3+}$ is well suited to react with a facially oriented $(NC)_3$ donor set provided by $[(Me_3tacn)Cr(CN)_3]$ or $[Cr(CN)_6]^{3-}$ to form the tetranuclear complex $[\mathbf{Mn_3Cr}]^{3+}$ and the heptanuclear complex $[\mathbf{Mn_6Cr}]^{3+}$, respectively. The bowl-shaped molecular structure of the triplesalen building block $[(talen^{t\text{-}Bu_2})\{Mn^{III}(solv)_n\}_3]^{3+}$ preorganizes the three Mn^{III} ions for the binding with the facially coordinated $(NC)_3$ donor set, thereby providing a driving force through molecular recognition. Problems in the preparation of $[\mathbf{Mn_3Cr}]^{3+}$ and its instability in MeOH solutions indicate a lower stability of $[\mathbf{Mn_3Cr}]^{3+}$ in comparison to $[\mathbf{Mn_6Cr}]^{3+}$. The molecular structure of $[\mathbf{Mn_6Cr}]^{3+}$ exhibits a significantly shorter $Mn-N^{N\equiv C}$ bond distance of 2.18 Å as compared to 2.29 Å in $[\mathbf{Mn_3Cr}]^{3+}$ and a stronger ligand folding at the central phenolate of 46.7° versus 35.8° in $[\mathbf{Mn_3Cr}]^{3+}$. Analysis in conjunction with other complexes identifies a supramolecular hydrophobic attraction between the two $[(talen^{t\text{-}Bu_2})Mn^{III}_3]^{3+}$ as a main source for the stronger ligand folding and thus the shorter $Mn-N^{N\equiv C}$ bond distances.

The small Hilbert space (500) enabled a thorough analysis of the temperature- and field-dependent magnetization data of $[\mathbf{Mn^{III}_3Cr^{III}}]^{3+}$ using the appropriate spin-Hamiltonian including zero-field splitting by a full-matrix diagonalization approach: $J_{Mn-Cr} = -0.12 \pm 0.04\ cm^{-1}$, $J_{Mn-Mn} = -0.70 \pm 0.03\ cm^{-1}$, $D_{Mn} = -3.0 \pm 0.4\ cm^{-1}$ with $g_{Cr} = g_{Mn} = 2.00$, and $D_{Cr} = 0\ cm^{-1}$. The shorter $Mn-N^{N\equiv C}$ bond in $[\mathbf{Mn_6Cr}]^{3+}$ results in a stronger antiferromagnetic J_{Mn-Cr} exchange coupling of $-5.0\ cm^{-1}$ versus $-0.12\ cm^{-1}$ in $[\mathbf{Mn_3Cr}]^{3+}$.

Despite the low J values, a spin manifold consisting of triply degenerate $|m_S = \pm 1/2\rangle$, $|m_S = \pm 3/2\rangle$, $|m_S = \pm 5/2\rangle$, and $|m_S = \pm 7/2\rangle$ Kramers doublets is energetically stabilized by $\sim 6\ cm^{-1}$. Although, these are the components of a total spin ground state of $S_t = 7/2$, the analysis shows that this in not a good quantum number, as strong field- and orientation-dependent mixings of the $|m_{s1},m_{s2},m_{s3},m_{s4}\rangle$ wave function occur. Thus, an analysis even of only the low-temperature magnetic data with a spin-Hamiltonian only describing the spin ground state (so-called effective spin model or giant-spin model) is not appropriate.

The field dependence of the low-lying energy states indicates a weak easy-axis magnetic anisotropy for $[\mathbf{Mn^{III}_3Cr^{III}}]^{3+}$, which is corroborated by the onset of frequency-dependent χ'' signals in the ac magnetization measurement in a zero dc field. This shows a slow relaxation of the magnetization indicative of $[\mathbf{Mn^{III}_3Cr^{III}}]^{3+}$ being a SMM.

This study has helped us to understand that supramolecular van der Waals type interactions between the two triplesalen ligands are the origin of the high driving force for the formation of our heptanuclear complexes $[\mathbf{M^t_6M^c}]^{n+}$, and to identify variations in the substituents of the triplesalen ligand as a good possibility to influence the $M^t-N^{N\equiv C}$ bond length, and therefore the $J_{M^t-M^c}$ exchange interaction, and thus finally the SMM properties.

Acknowledgment. This work was supported by the DFG (FOR945 "Nanomagnets: from Synthesis via Interactions with Surfaces to Function"), the Fonds der Chemischen Industrie, Bielefeld University, and NSF Grant No. CHE-0617063. We thank the Natural Sciences and Engineering Council of Canada for support of M.W.D., and we are grateful to Dr. Eckhard Bill (Max-Planck-Institute for Bioinorganic Chemistry, Mülheim, Germany) for supplying us with a personalized version of the program package julX.

Supporting Information Available: A crystallographic information file and a file with additional figures are available. This material is available free of charge via the Internet at http://pubs.acs.org.